RSC Advances

PAPER

View Article Online
View Journal | View Issue

Cite this: *RSC Adv.*, 2023, **13**, 14660

Multifunctional optical thermometry using dual-mode green emission of $CaZrO_3$:Er/Yb/Mo perovskite phosphors

Hoang Tuan Nam,[a] Phuong Dinh Tam,[a] Nguyen Van Hai[b] and Hoang Nhu Van *[a]

The weak emission intensity of rare-earth element-doped dual-mode materials leads to low-sensor sensitivity, which is a challenge in optical sensor applications. The present work achieved high-sensor sensitivity and high green color purity based on the intense green dual-mode emission of Er/Yb/Mo-doped $CaZrO_3$ perovskite phosphors. Their structure, morphology, luminescent properties, and optical temperature sensing properties have been investigated in detail. Phosphor shows a uniform cubic morphology with an average size of approximately 1 μm. Rietveld refinement confirms the formation of single-phase orthorhombic $CaZrO_3$. Under the excitation of 975 and 379 nm, the phosphor emits pure green up and down-conversion (UC and DC) emission at 525/546 nm corresponding to $^2H_{11/2}/^4S_{3/2}-^4I_{15/2}$ transitions of Er^{3+} ions, respectively. Intense green UC emissions were achieved because of energy transfer (ET) from the high-energy excited state of $Yb^{3+}-MoO_4^{2-}$ dimer to the $^4F_{7/2}$ level of Er^{3+} ion. Furthermore, the decay kinetics of all obtained phosphors confirmed ET efficiency from $Yb^{3+}-MoO_4^{2-}$ dimer to Er^{3+} ions, leading to strong green DC emission. Moreover, the DC of the obtained phosphor shows that a sensor sensitivity value of 0.697% K^{-1} at 303 K is higher than the UC (0.667% K^{-1} at 313 K) because the thermal effect generated by the DC excitation source light is ignored compared with UC luminescence. $CaZrO_3$:Er–Yb–Mo phosphor shows intense green dual-mode emission with high green color purity, 96.50% of DC and 98% of UC emissions, and high sensitivity, making it suitable for optoelectronic devices and thermal sensor applications.

Received 26th April 2023
Accepted 9th May 2023

DOI: 10.1039/d3ra02759g

rsc.li/rsc-advances

1. Introduction

Temperature is an essential physical parameter in science and daily life; thus, the accurate measurement of temperature is critical.[1,2] However, conventional contact temperature measurement using liquid-filled glass thermometers and thermocouples has many disadvantages, such as low sensitivity, limitation in response time, and inability to measure under harsh conditions (such as high temperature, strong acids, and strong magnetic fields).[3,4] Thus, the temperature sensor application of this method is hindered.[3] At present, non-contact temperature measurement methods *via* optical temperature sensors based on temperature-dependent up and down-conversion (UC and DC) emission intensity are widely used because they could overcome the limitations of conventional contact temperature measurement.[5,6] Accordingly, several parameters of rare-earth (RE) element-doped phosphors, such as emission intensity, lifetime, and peak shift, depend on temperature,[7] which is used for determining temperature sensing sensitivity.[7,8] Notably, the fluorescence intensity ratio (FIR) based on the emission spectra of the phosphor is widely used to estimate the sensor characteristics of phosphors. This technique is performed by observing the changing intensity emission of two thermally coupled levels of RE ions with an energy gap from 200 to 2000 cm^{-1}.[8] The FIR is independent of an activator, spectrum losses, and fluctuation in excitation intensity.[9] Therefore, this method has good measurement accuracy, high resolution, and broad range, and it requires low excitation power, leading to high reliability.[9,10] However, previous literature reports only explore the sensor sensitivity of a single UC or DC material instead of both. In addition, DC emission shows that a thermal effect generated by the excitation light could be ignored, resulting in high sensor sensitivity.[6] Therefore, investigating the sensor sensitivity based on UC and DC emissions is necessary to extend the application of phosphors.

Er^{3+} ion is a widely used activator for UC/DC luminescent materials. It has an energy gap between $^2H_{11/2}$ and $^4S_{3/2}$ levels of approximately 800 cm^{-1},[11] indicating that it is suitable as a luminescent center for phosphor-temperature sensor using the FIR.[11,12] However, due to small absorption cross-section in the near-infrared band led to its low emission intensity.[13]

[a]*Faculty of Materials Science and Engineering, Phenikaa University, Yen Nghia, Ha-Dong District, Hanoi 12116, Vietnam. E-mail: van.hoangnhu@phenikaa-uni.edu.vn*

[b]*Faculty of Chemistry, Hanoi National University of Education, 136 Xuan Thuy Road, Cau Giay District, Hanoi, Vietnam*

Previous works showed that weak UC emission intensity of phosphors results in low sensor sensitivity, which could not be suitable for temperature sensor applications.[13,14] Recently, researchers have achieved good temperature sensing properties based on a selective enhancement of green UC emission using a sensitizer pair as Yb^{3+}-transition metal (TM) to activate Er^{3+}.[15,16] Energy transfer at a high-energy excitation state of the Yb^{3+}-TM ion pairs to the $^4F_{7/2}$ level of Er^{3+} could reduce non-radiative transition and improve UC efficiency and sensor sensitivity. B. Dong *et al.* have reported that high-temperature sensor sensitivity was achieved by using Yb^{3+}–MoO_4^{2-} dimer sensitizer to activate Er^{3+} on $Yb_3Al_5O_{12}$ (ref. 17) and Al_2O_3 (ref. 16) host lattices. Meanwhile, X. Yang *et al.*[18] have observed an intense green UC emission of Er–Yb-doped $NaY(MoO_4)_2$ phosphor with good temperature sensing properties, thereby causing ET from Yb^{3+}–MoO_4^{2-} dimer to Er^{3+}. Besides, the MoO_4^{2-} groups (obtained by Mo^{6+} doped host) have a high absorption cross-section at the UV region; thus, they can strongly absorb radiation in this region and transfer energy to the RE doping ion, resulting in an improvement in the RE ion's emission efficiency.[19] Furthermore, the presence of the Mo^{6+} ion in the host lattice leads to a decrease in the lattice symmetry and enhances stark energy splitting in the crystal field because they have a short radius and large electric charge, enabling a powerful polarization effect.[19,20] Most recently, our previous works explored the super enhancement of green UC emission by using the Yb^{3+}–MoO_4^{2-} dimer sensitizer for Er^{3+} ion on HA/TCP (650 times)[21] and HA (70 times),[22] thereby achieving good temperature sensing properties in BCP host.[23] Based on previous works, the strong green UC emission of phosphors can be achieved by using Er–Yb–Mo tri-doped systems, leading to the enhancement of sensing sensitivity.[15,23] Furthermore, several works[1,3,23,24] have observed that temperature sensitivity depends on the host lattice.

Oxides are widely used for luminescent hosts because of their excellent properties, such as low phonon energy, high thermal stability, and wide-range transparency.[7] The perovskite-type oxide $CaZrO_3$ has an orthorhombic structure with space group *Pbnm*, and it has received considerable attention as a host material because of its excellent physical–chemical properties.[25,26] It has relatively low phonon energy, resulting in reduced non-radiative transition, thereby enhancing UC and DC efficiency. A. Khan *et al.*[27] successfully prepared Dy^{3+}/Eu^{3+}/Mo^{6+}-doped $CaZrO_3$ for white light emission through a solid-state reaction at 1200 °C for 6 h. V. Singh *et al.*[28] reported the intense green and red UC emission of Er–Yb-doped $CaZrO_3$ by solution combustion. A. Maurya *et al.*[29] investigated the effect of alkali ions on optical properties, and the temperature sensing efficiency of Er–Yb-doped $CaZrO_3$ was prepared by a solid-state reaction. They found that the enhancement of UC emission of the systems by adding alkali ions was caused by a change in the local crystal field and an increase the crystallinity of the obtained phosphors. The RE-doped $CaZrO_3$ host lattice was successfully prepared in previous works.[30,31] However, to our knowledge, the intense green UC and DC emission of $CaZrO_3$:Er/Yb/Mo phosphor with good optical temperature sensing properties has yet to be well documented.

Table 1 Labels of all investigated samples

Materials	Mo^{6+} content (mol%)	Label
1Er–10Yb doped $CaZrO_3$	0	S0
1Mo–1Er–10Yb doped $CaZrO_3$	1	S1
3Mo–1Er–10Yb doped $CaZrO_3$	3	S3
5Mo–1Er–10Yb doped $CaZrO_3$	5	S5
8Mo–1Er–10Yb doped $CaZrO_3$	8	S8

Herein, $CaZrO_3$:Er/Yb/Mo microstructure phosphors with good sensor sensitivity are synthesized *via* a solid-state reaction. Their structure, morphology, and optical property were investigated in detail. The optical temperature sensing was characterized using the FIR. Their characteristics were analyzed using X-ray diffraction (XRD), high-resolution scanning electron microscopy (FE-SEM), photoluminescence (PL), and FIR.

2. Experimental

1% Er, 10% Yb, and x% Mo ($x = 0$, 1, 3, 5, and 8% mol) co-doped $CaZrO_3$ phosphors were prepared through a solid-state reaction. $Er(NO_3)_3 \cdot 5H_2O$ (99.99%), $Yb(NO_3)_3 \cdot 5H_2O$ (99.99%), $(NH_4)_6Mo_7O_{24}$ (99.9%), ZrO_2 (99.9%), and $CaCO_3$ (99.9%) were utilized as precursors. The precursors were ground using an agate mortar for 1 h and then treated at 500 °C for 5 h. Next, the powder mixture was ground again for 1 h and incubated at 900 °C for 5 h. Finally, the homogeneous powders were further calcined at 1300 °C for 5 h. All investigated samples were labeled (Table 1).

Their structural property was characterized using an X-ray diffractometer (Bruker D8 Advance). Their morphological property was analyzed using high-resolution scanning electron microscopy (JEM 1010, JEOL Technique, Japan). Diffuse reflectance spectra were recorded using a Varian Cary 5000 UV-vis-NIR spectrophotometer. The luminescence properties of UC and DC were recorded using a NANO LOG spectrometer (Horiba, USA) equipped with a 975 nm laser radiation source and heat controller. The Rietveld refinement structure of phosphors was obtained using FullProf software.

3. Results and discussion

3.1. XRD analysis

Fig. 1a shows the XRD pattern of all investigated samples $CaZrO_3$:Er–Yb without and with Mo-doped. Diffraction peaks of all patterns match well with the standard card (PDF # 00-061-0228) of orthorhombic single-phase $CaZrO_3$ with a *Pbnm* space group. Their intensity is sharp and strong, which indicates the high crystallinity of phosphors. Moreover, diffraction peaks intensity tends to increase with rise of Mo^{6+} doping content up to 3% mol, then slight decrease with higher Mo^{6+} content. These results confirm the presence of Mo^{6+} ion influency on structure and crystallinity of the host lattice. The structure of orthorhombic $CaZrO_3$ includes CaO_8 polyhedra and ZrO_6 octahedra, with the following lattice parameters (Fig. 1b): $a = 5.60$ Å,

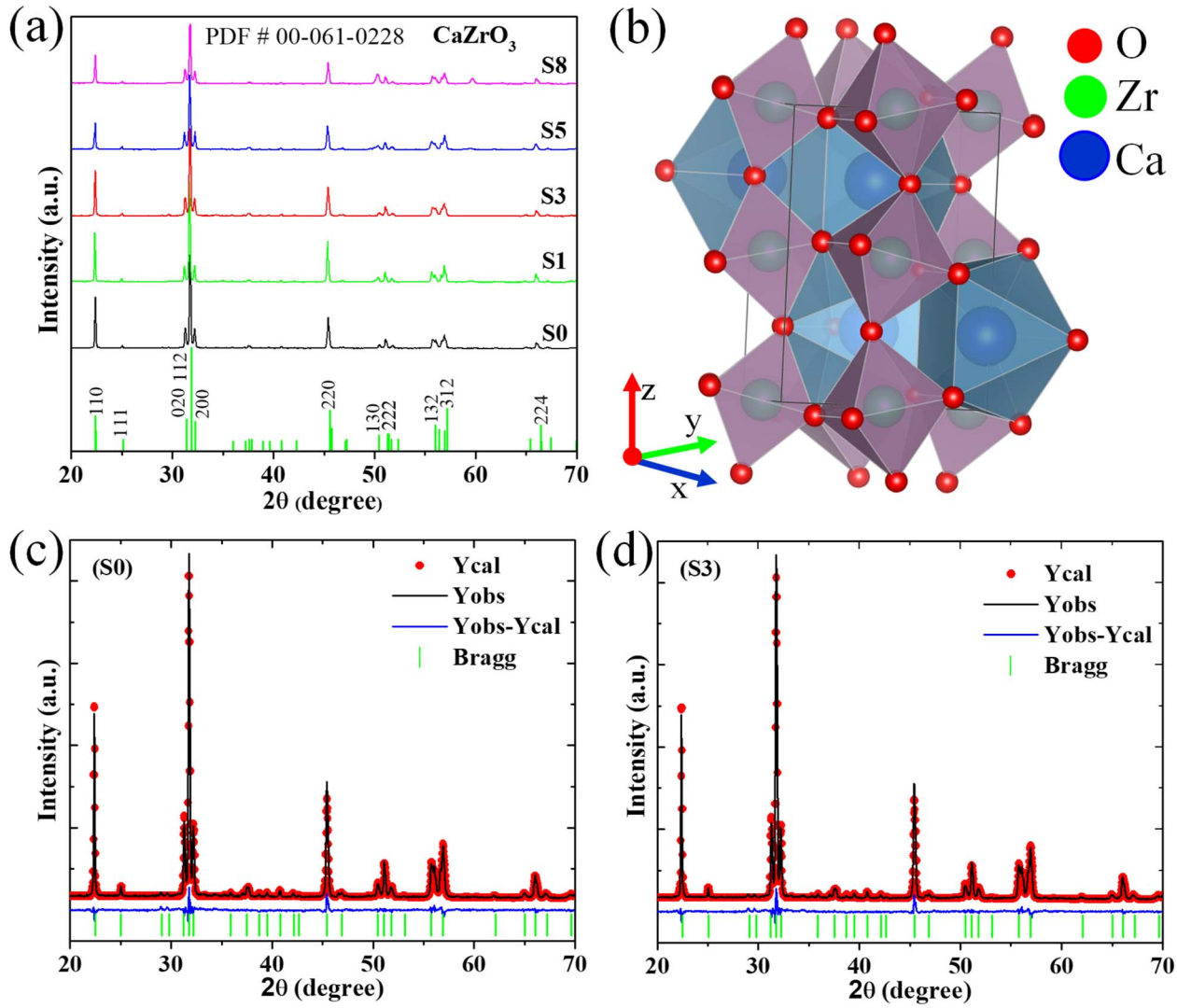

Fig. 1 (a) XRD pattern of all investigated samples; (b) crystal structure of $CaZrO_3$ from Rietveld refinement; (c) and (d) Rietveld refinement structure of the typical samples S0 and S3.

Table 2 Lattice parameters from Rietveld refinement of samples S0 and S3[a]

Parameter	$CaZrO_3$:Er–Yb	$CaZrO_3$:Er–Yb–Mo
Space group	*Pbnm*	*Pbnm*
Symmetry	Orthorhombic	Orthorhombic
a, Å	5.5948	5.5938
b, Å	5.7554	5.7556
c, Å	8.0190	8.0170
V, Å^3	258.2139	258.1129
R_{exp} (%)	4.65	4.65
R_p (%)	6.20	6.08
R_{wp} (%)	7.58	7.06
GOF	2.65	2.30

[a] GOF = $(R_{wp}/R_{exp})^2$.

b = 5.75 Å, and c = 8.01 Å. On the other hand, according to A. Khan *et al.*,[27] the difference in ionic radii between doped and substituted ions with an acceptable percentage was lower than 30%. In this case, the radius percentage (D_r) between the doped ions (Er^{3+}, Yb^{3+}, and Mo^{6+}) and the substituted ions (Ca^{2+} and Zr^{4+}) in $Ca_{1-x-y}Zr_{1-z}O_3$:xEr^{3+}, yYb^{3+}, zMo^{6+} was determined using eqn (1):[27,32]

$$D_r = \frac{R_s(CN) - R_d(CN)}{R_s(CN)} \quad (1)$$

where CN = 6 is the coordination number of the resulted ions. R_s(CN) and R_d(CN) are radius of the substituted and dopant ions, respectively. The ionic radius values such as Er^{3+} (0.89 Å), Yb^{3+} (0.87 Å), Mo^{6+} (0.60 Å),[21] Zr^{4+} (0.72 Å), and Ca^{2+} (0.99 Å) can be taken from the literature.[27] According to eqn (1), the D_r values were calculated to be $D_r(Er^{3+}/Ca^{2+})$ 10%, $D_r(Yb^{3+}/Ca^{2+})$ 12%, and $D_r(Mo^{6+}/Zr^{4+})$ 17%. In contrast, the $D_r(Mo^{6+}/Ca^{2+})$ value is 39.4% that is much higher than 30%. Therefore, these results indicate that Er^{3+} and Yb^{3+} are substitute Ca^{2+} sites. Meanwhile, Mo^{6+} is substitute Zr^{4+} sites, which agree with the Rietveld refinement result in Table 2.

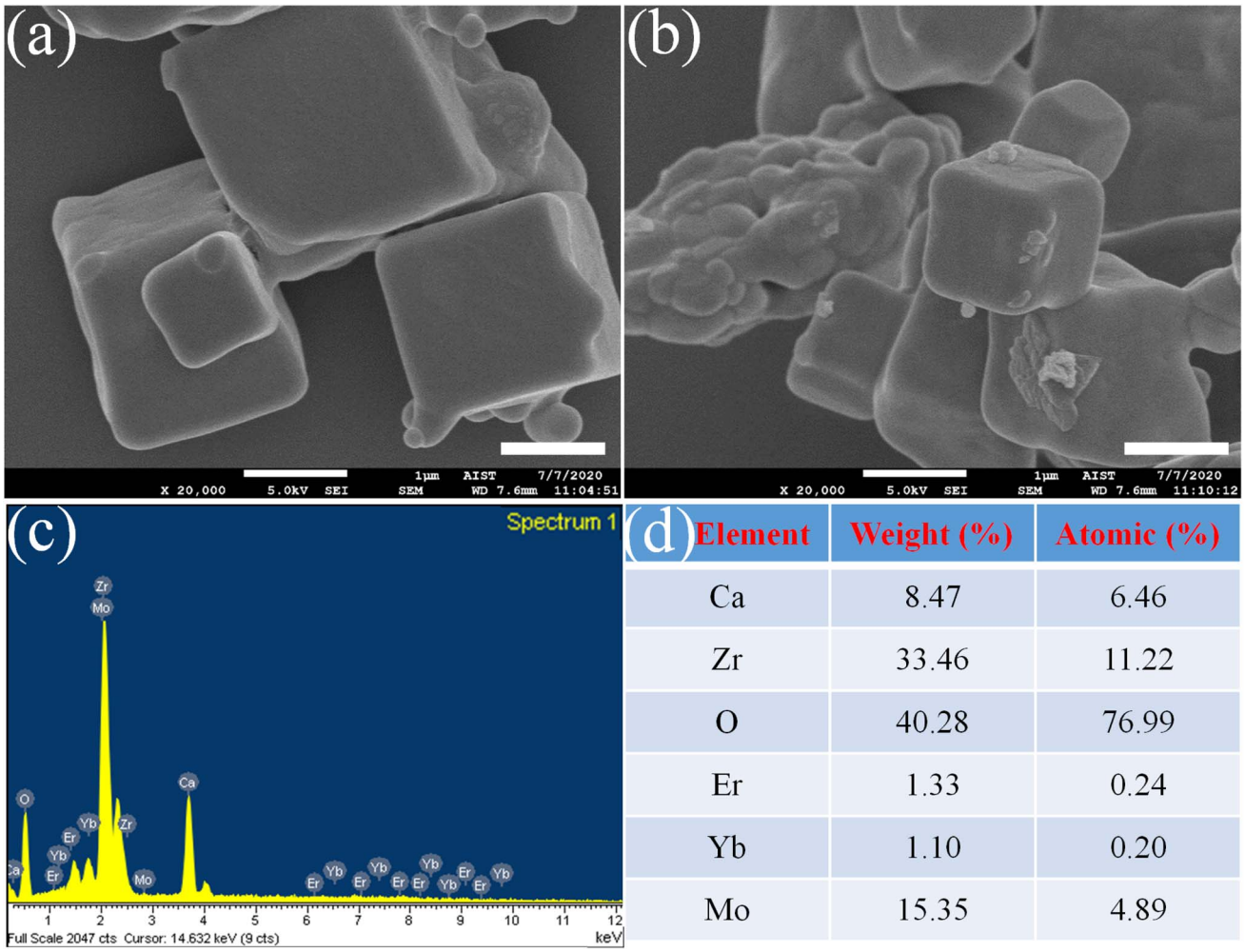

(d)

Element	Weight (%)	Atomic (%)
Ca	8.47	6.46
Zr	33.46	11.22
O	40.28	76.99
Er	1.33	0.24
Yb	1.10	0.20
Mo	15.35	4.89

Fig. 2 FE-SEM images of (a) S0 and (b) S3 (scale bar of 1 μm), (c) EDS spectra, and (d) element percentage of the investigated sample S3.

Furthermore, to confirm the influence of Mo^{6+} doped in the crystal structure of the material, the Rietveld refinement of the typical two samples (S0 and S3) was performed using the standard card PDF # 00-061-0228 as references (Fig. 1c and d). As shown in Fig. 1c and d, the experimental result is consistent with the calculated results, indicating the reliability of the refinement technique, and all refinement parameters (as atom coordinates, fraction factors, and thermal vibration) are consistent with the reflection condition.[33] As shown in Table 2, the change in lattice parameters (*a*, *c*, and *V*) of sample S3 compared with sample S0 confirms the successful replacement of Mo^{6+} for Zr^{4+} sites into the host lattice. In addition, impurity phases were not observed in all samples, indicating the successful synthesis of the resulting phosphors.

3.2. SEM and EDS analysis

Fig. 2a and b show FE-SEM images of samples S0 and S3. All samples show a cubic grain morphology with a uniform distribution and clear grain boundary. The sample S0 exhibits a grain size of approximately 1.2 μm (Fig. 2a), whereas the doped sample (S3) is approximately 1 μm (Fig. 2b), which is due to the

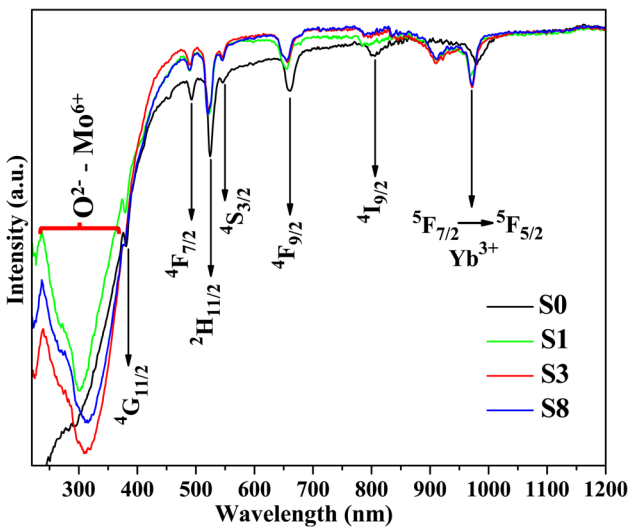

Fig. 3 Diffuse reflectance spectra of investigated samples S0, S1, S3, and S8.

substitution of small ionic radius (Mo^{6+}, 0.6 Å) for larger ionic radius (Zr^{4+}, 0.72 Å).[27] Meanwhile, Fig. 2c shows resulting peaks corresponding to Ca, O, Zr, Er, Yb, and Mo with element percentage (Fig. 2d) from elemental analysis of the EDS spectrum, indicating the presence of Er, Yb, and Mo doped in $CaZrO_3$ host lattice. In addition, as shown in Fig. 2c and d, other impure chemical elements were not observed, indicating the high purity of the investigated phosphors in this work. These results indicate the high crystallinity degree of resulting phosphor, which is consistent with the XRD results shown in Fig. 1a, leading to the improvement of UC efficiency of the phosphor.

3.3. Optical characteristics

3.3.1. DRS spectral measurements. Fig. 3 shows the diffuse reflectance spectra of samples S0, S1, S3, and S8. As shown in Fig. 3, broad absorption bands from 230 to 350 nm are attributed to the O^{2-}–Er^{3+}/Yb^{3+}/Mo^{6+} charge transfer band.[34] Significantly, these absorption band intensity increases with the rise of Mo^{6+} doping content due to the covalency of the Mo–O bond being higher than that of the Zr–O bond because of the difference in electronegativity between the Mo^{6+} (2.16) and the Zr^{4+} (1.4),[35] which confirms the presence of Mo^{6+} ion in the host. It can be seen in Fig. 3 typical sharp absorption bands such as 380, 492, 524, 546, 660, and 805 nm correspond to transitions from the $^4I_{15/2}$ level to $^4G_{11/2}$, $^4F_{7/2}$, $^2H_{11/2}$, $^4S_{3/2}$, $^4F_{9/2}$, and $^4I_{9/2}$ levels of Er^{3+} ion. Meanwhile, the broad absorption band at NIR (around 975 nm) corresponded to an overlap between the $^5F_{7/2}$–$^5F_{5/2}$ transition of Yb^{3+} ions and the $^4I_{15/2}$–$^4I_{11/2}$ transition of Er^{3+} ions. These results confirm the successful introduction of Er^{3+} and Yb^{3+} ions into the $CaZrO_3$ host lattice. Significantly, the absorption peaks of doped samples (S1, S3, and S8) are blue shifted compared with the undoped sample (S0), which is due to the difference between the ionic radius of the dopant and the host cation,[36] indicating the presence of Mo^{6+} dopant ions on the host lattice and leading to the formation of Yb^{3+}–MoO_4^{2-} dimers in the system. These results supported the proposed energy level diagram of the Er–Yb–Mo-doped $CaZrO_3$ phosphor (Fig. 6).

3.3.2. UC luminescence properties. Fig. 4a shows UC emission spectra of all samples doped with various Mo^{6+} contents.

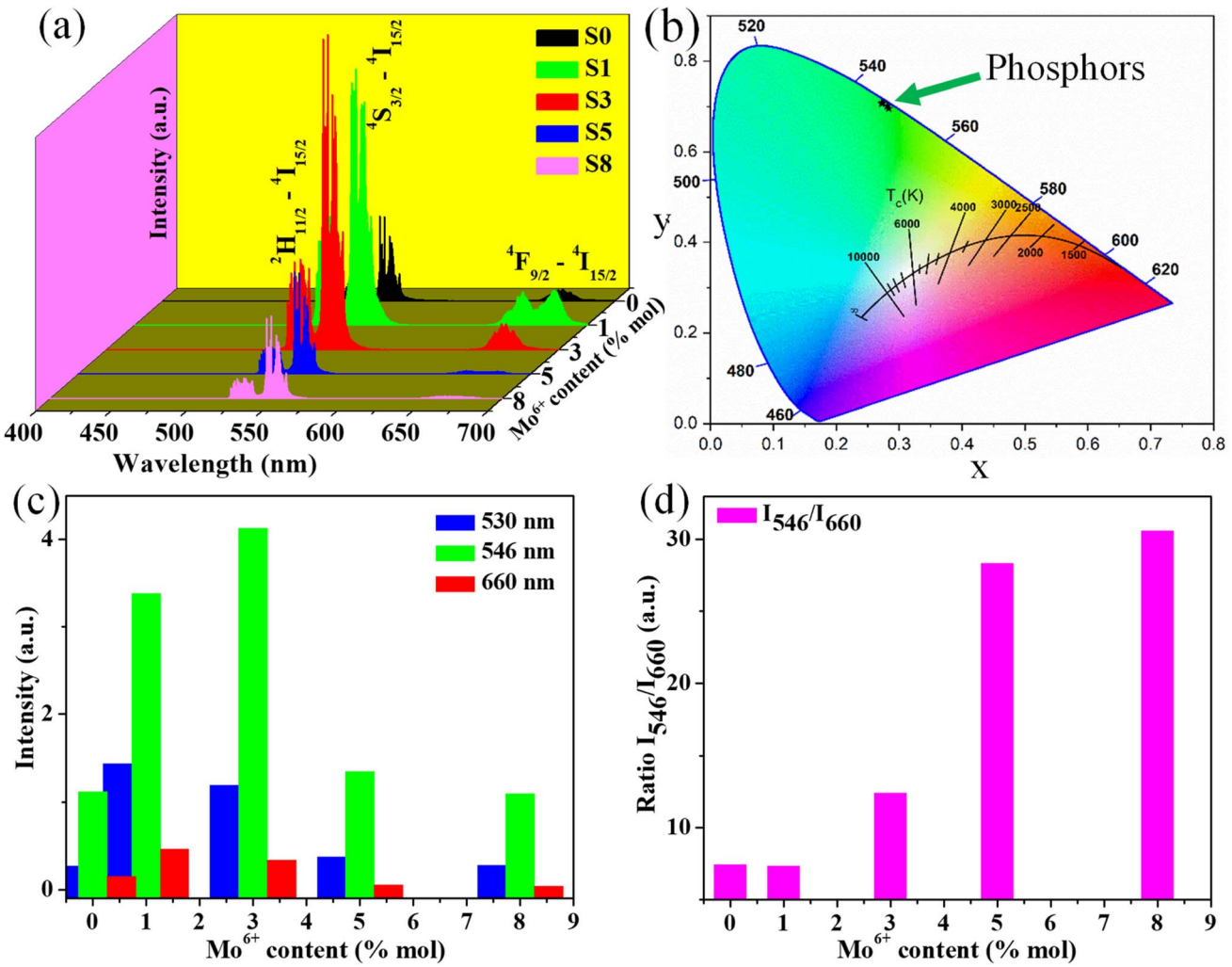

Fig. 4 (a) UC spectra of all samples with various Mo^{6+} content doping, (b) CIE chromaticity coordinates of all UC emission samples, (c) UC emission intensity of all samples as a function of Mo^{6+} doping content, and (d) I_{546}/I_{660} intensity ratio of all samples.

Table 3 The CIE chromaticity coordinates and color purity of different samples

Samples	Chromaticity coordinates (x, y)	Color purity (%)
S0	(0.2835, 0.6964)	93.11
S1	(0.2809, 0.7012)	94.41
S3	(0.2743, 0.7084)	96.50
S5	(0.2722, 0.7076)	96.35
S8	(0.2721, 0.7070)	96.21

As shown in Fig. 4a, under excitation of 975 nm, all samples exhibit two typical emission bands: (i) strong green emission bands at 525/546 nm are attributed to the $^2H_{11/2}/^4I_{3/2}$–$^4I_{15/2}$ transition of Er^{3+} ion; (ii) the weak red emission band at 660 nm is due to the $^4F_{7/2}$–$^4I_{15/2}$ transition of Er^{3+} ion. Green and red emission intensities depend on the Mo^{6+} doping content and reach the maximum intensity of 3% mol Mo^{6+} (Fig. 4c). By adding Mo^{6+} ion into the system, the green emission intensity of the phosphor has been enhanced up to fourfold. The energy transfer effectively process from the high-energy excited state ($|^2F_{7/2}$, $^3T_2$)) of the Yb^{3+}–MoO_4^{2-} dimer to the $^4F_{7/2}$ level of the Er^{3+} ion is responsible for the strong green emission of phosphors.[15,23,37] When Mo^{6+} doping content is higher than 3% mol, the UC emission intensity decreases because of the energy migration between Yb^{3+}–MoO_4^{2-} dimers[23,37] and between the MoO_4^{2-} groups as a donor in the energy transfer process.[38] On the contrary, the weak absorption cross-section of the $^4I_{13/2}$ state of the Er^{3+} ions led to weak red emission intensities. Moreover, the dominant UC ET process leads to the transfer of electrons from the $^4I_{11/2}$ level to the $^4F_{7/2}$ level, which is higher than that of non-radiative relaxation to the $^4I_{13/2}$ level formation of weak red emission (Fig. 6). Furthermore, the green/red (I_{546}/I_{660}) intensity ratio of all samples increased with enhanced Mo^{6+} doping content, indicating remarkable control-enhanced green emission using Mo^{6+} doping ions (Fig. 4d).

Additionally, Commission International de l'Eclairage (CIE) chromaticity coordinates of investigated samples were

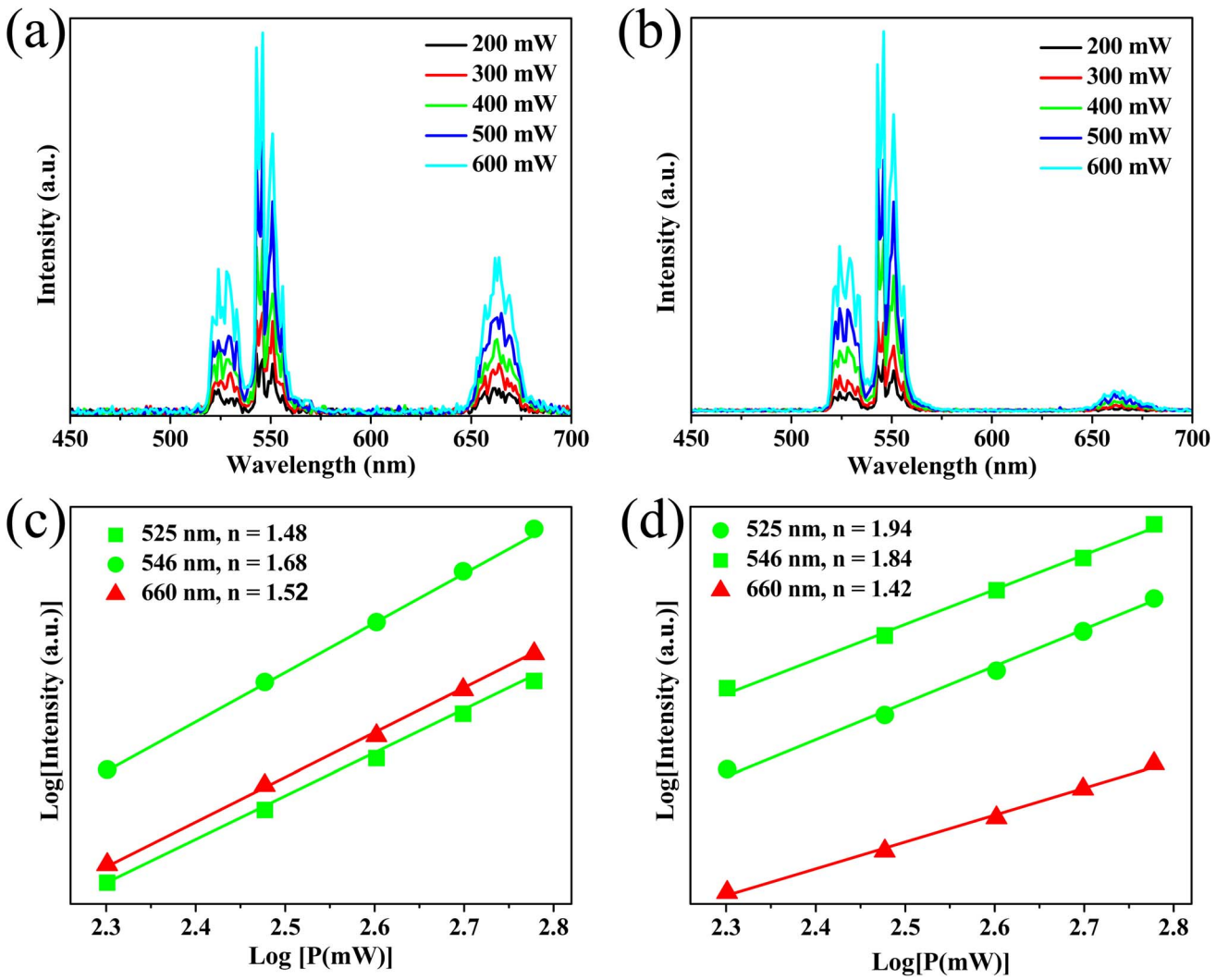

Fig. 5 Emission intensity-dependent excitation power of the samples S0 (a) and S3 (b) and the log–log plots of green/red emission as a function of the power of the samples S0 (c) and S3 (d).

calculated from their emission spectra presented in Fig. 4b. In this case, the obtained values of all samples are displayed in Table 3. As shown in Table 3, the chromaticity coordinates value of the S3 sample (0.2743, 0.7084) is close to the standard green chromaticity coordinated for the National Television Standard Committee (NTSC) system.[39] Significantly, the color purity of the green light emission phosphors in this work was calculated using eqn (2):[40]

$$\text{Color purity} = \frac{\sqrt{(x-x_i)^2+(y-y_i)^2}}{\sqrt{(x_d-x_i)^2+(y_d-y_i)^2}} \times 100\% \quad (2)$$

where (x, y) present the color coordinates of samples; $x_i = 0.3333$ and $y_i = 0.3333$ correspond to the color coordinate of the white light source; (x_d, y_d) means the color coordinates of the dominant wavelength.[39] Putting these values (x, y), (x_i, y_i), and (x_d, y_d) into eqn (2), the color purity of resulted samples is exhibited in Table 3. Notably, the color purity of samples increased with enhanced Mo^{6+} doping content and reached a maximum value of 96.50% (S3 sample), indicating pure green light emission. This result suggests the potential application of phosphor for optoelectronic devices. Consequently, the S3 sample with the highest emission intensity was selected to analyze the temperature sensor properties.

3.3.3. UC emission mechanism. The intense green UC emission mechanism (S0 and S3 samples) of the obtained phosphor can be explained through the relationship between the emission intensity (I) and excitation power (P) as[41] $I \propto P^n$, where n is the number of photons absorbed for emitter UC. Fig. 5a and b show that I increase rapidly with the increase of P from 200 to 600 mW of the two samples (S0 and S3). In sample S0 (Fig. 5c), the slope values (n) are 1.48/1.68 and 1.52, corresponding to the $^2H_{11/2}/^4I_{3/2}$–$^4I_{15/2}$ (green) and $^4F_{7/2}$–$^4I_{15/2}$ (red) transitions, respectively. In sample S3, the corresponding slopes are 1.94/1.84 and 1.42 (Fig. 5d). These results indicate the two-photon process for green/red emissions of the two obtained

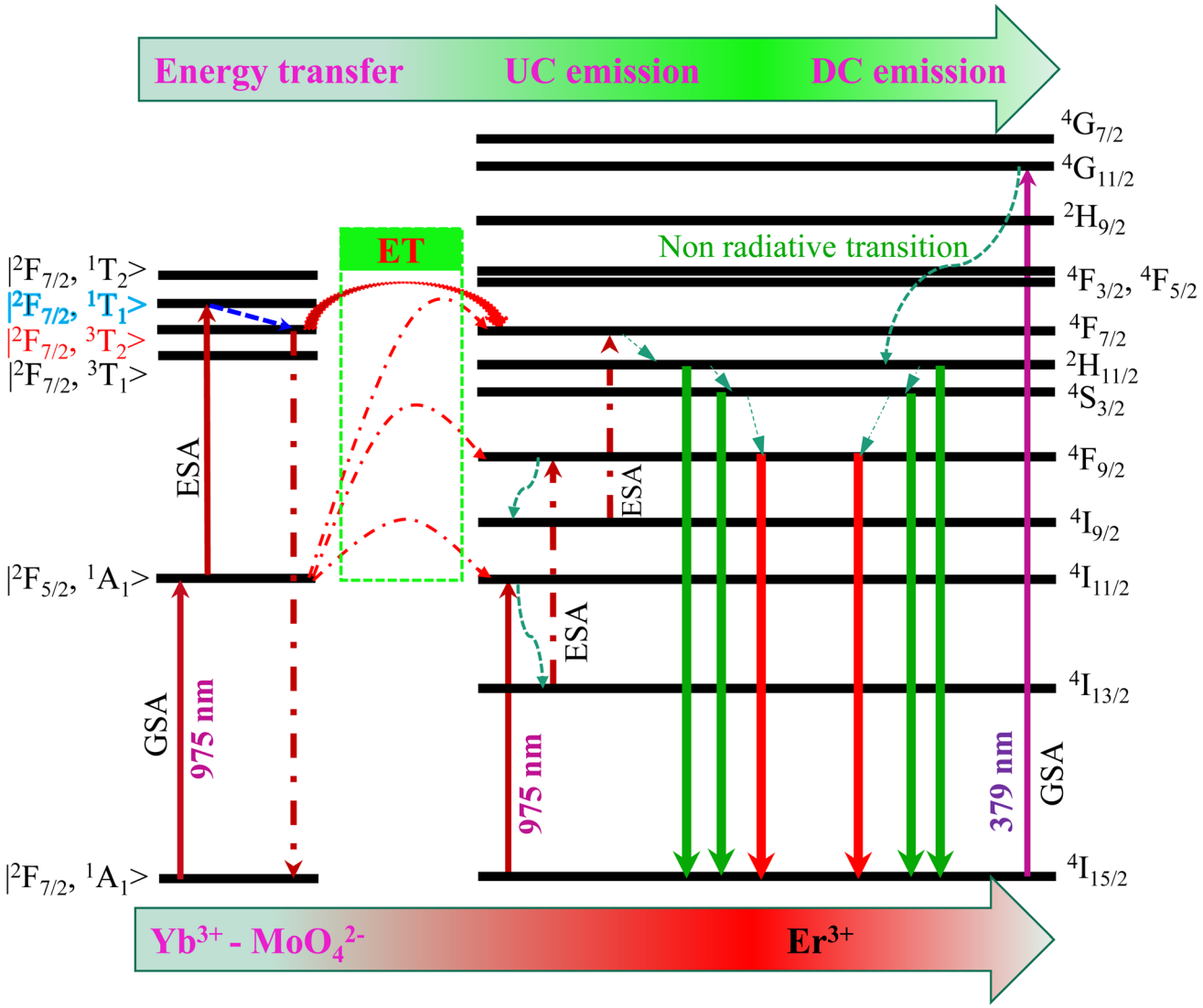

Fig. 6 Energy level diagram of Er/Yb/Mo doped $CaZrO_3$ phosphor.

samples. Significantly, the n values corresponding to the green emission of sample S3 are higher than that of the S0 sample. By contrast, the n value of red emission is low, which confirms the effective ET from the Yb^{3+}–MoO_4^{2-} dimer to the Er^{3+} ions, thereby enhancing green UC emission. This result was further used to build the energy level diagram and explain the UC emission mechanism (Fig. 6).

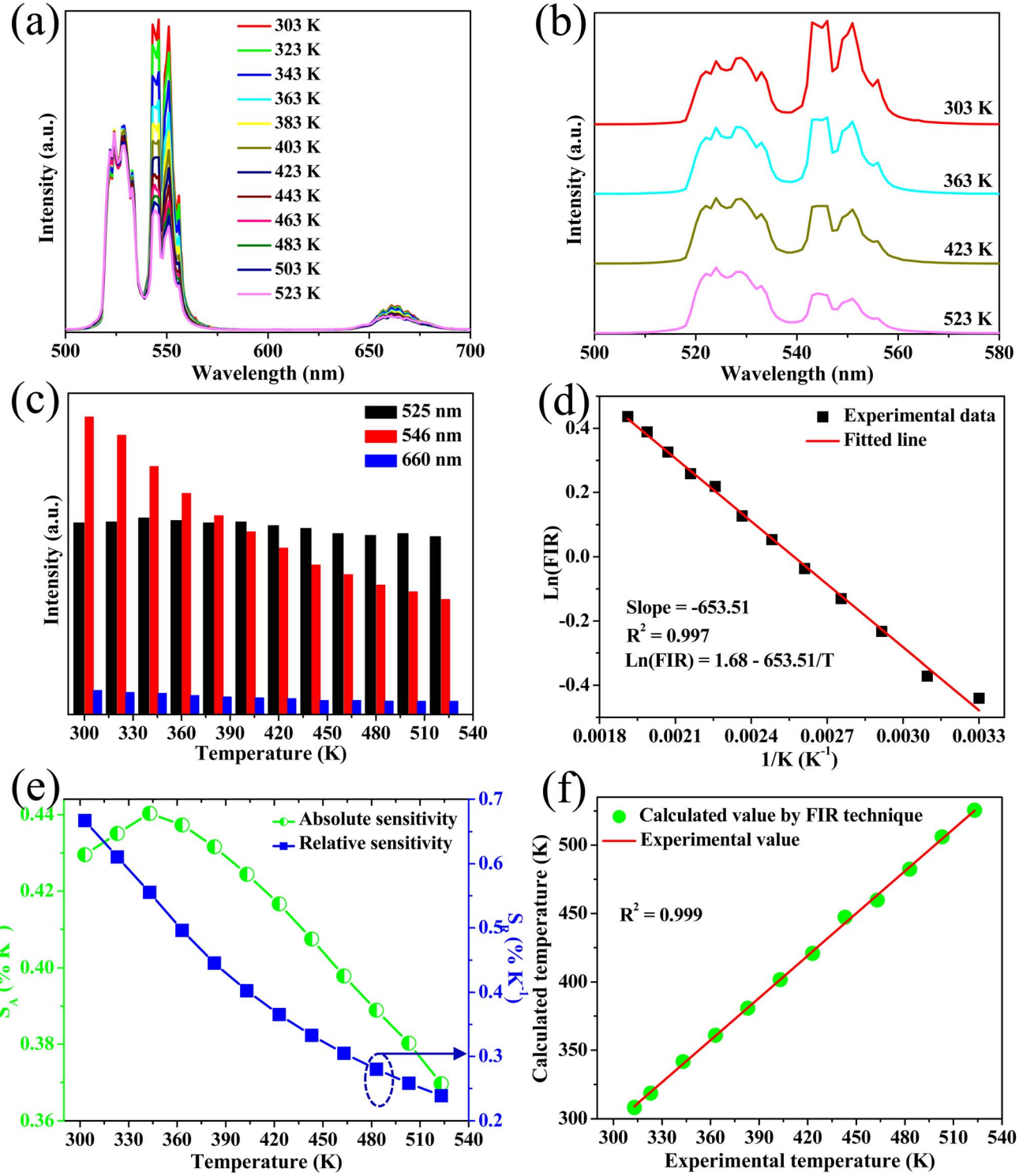

Fig. 7 (a) Green/red emission spectra of the S3 sample measured from 313 K to 523 K, (b) comparison of green emission of the S3 sample at several temperatures, (c) greed/red emission intensity as a function of temperature, (d) the relationship between the ln(FIR) value and inverse absolute temperature, (e) the sensitivity (absolute and relative) value of the sample using the FIR, and (f) the relationship between calculated and experimental temperature.

3.3.4. Energy level diagram of UC and DC green emission of Er–Yb–Mo tri-doped $CaZrO_3$ phosphor. In understanding the selective enhancement of green UC emission, the energy level diagram of the CZO:Er–Yb–Mo system is schematically explained in Fig. 6. The intense green UC emission (in the S3) of the system can be discussed using three main processes: ground-state absorption (GSA), excited-state absorption (ESA), and ET.[42] For doped samples, GSA, ESA, and ET are responsible for the sensitizer of the Yb^{3+}–MoO_4^{2-} dimer. The dominant green emission of $CaZrO_3$:Er–Yb–Mo is proposed as follows:

➢ Step 1: the energy level of the Yb^{3+}–MoO_4^{2-} dimer, such as $|^2F_{7/2}, {}^1A_1\rangle$ (ground state), $|^2F_{5/2}, {}^1A_1\rangle$ (excited state), and $|^2F_{7/2}, {}^3T_1\rangle$, $|^2F_{7/2}, {}^3T_2\rangle$, $|^2F_{7/2}, {}^1T_1\rangle$, $|^2F_{7/2}, {}^1T_2\rangle$ (at highly excited state), was obtained by mixing the electron wavefunctions of Yb^{3+} and MoO_4^{2-}.[43]

➢ Step 2: the electron at the initial state $|^2F_{7/2}, {}^1A_1\rangle$ of the Yb^{3+}–MoO_4^{2-} dimer absorbs one photon, and it is excited to the $|^2F_{5/2}, {}^1A_1\rangle$ level *via* GSA.

➢ Step 3: the electron at the $|^2F_{5/2}, {}^1A_1\rangle$ level absorbs a second photon, and then they are elevated to the $|^2F_{7/2}, {}^1T_1\rangle$ level (high-energy excited state) by ESA. Given the unstable $|^2F_{7/2}, {}^1T_1\rangle$ state, leading to the non-radiative relaxation of the electron to the $|^2F_{7/2}, {}^3T_2\rangle$ state.

➢ Step 4: the electron at $|^2F_{7/2}, {}^3T_2\rangle$ state ET to $^4F_{7/2}$ level of Er^{3+} and then relax NR down to two meta-stable levels, $^2H_{11/2}/^4S_{3/2}$. Next, most of the electrons in $^2H_{11/2}$ and $^4S_{3/2}$ levels return to the ground-state $^4I_{15/2}$, producing intense green emission (530/546 nm).

Meanwhile, the red emission is originally from the $^4F_{7/2}$ NR to the $^4S_{3/2}$ level. However, the $^4S_{3/2}$ energy level is higher than the $^4F_{9/2}$ level, leading to a few electrons from the $^4S_{3/2}$ NR to the $^4F_{9/2}$ level,[37] causing red emission that is weaker (several orders of magnitude) than green emission. These results are used to explain the experimental evidence shown in Fig. 4a. Thus, the proposed mechanism for the intense green UC emission is suitable.

3.4. Optical temperature sensing characterization based on UC emission

The potential application in temperature sensors of the phosphor was evaluated by determining the temperature-dependent green UC emission of the S3 sample. The Er^{3+} ion has two thermal coupled levels, $^2H_{11/2}/^4S_{3/2}$, with an energy gap of approximately ~800 cm^{-1}.[44] Thus, the thermal equilibrium between these two levels can be achieved through thermal excitation. Fig. 7a shows the UC emission of the S3 sample under different temperatures ranging from 303 K to 523 K. The emission intensities of samples decrease with the increase of temperature. Notably, the emission intensity of the $^4S_{3/2}$–$^4I_{15/2}$ transition rapidly decreases. Meanwhile, the $^2H_{11/2}$–$^4I_{15/2}$ and $^4F_{7/2}$–$^4I_{15/2}$ transitions slightly change, indicating the excellent thermal stability of the phosphor.

Based on the FIR technique, the emission intensity ratio corresponding to $^2H_{11/2}$–$^4I_{15/2}/^4S_{3/2}$–$^4I_{15/2}$ transitions was used to estimate the optical temperature sensor characteristics of the phosphor using eqn (3):[45]

$$\mathrm{FIR} = \frac{I_{525}}{I_{546}} = A e^{-\frac{\Delta E}{kT}} \quad (3)$$

where I_{525} and I_{546} are the emission intensities corresponding to the $^2H_{11/2}$–$^4I_{15/2}/^4S_{3/2}$–$^4I_{15/2}$ transitions; A is a pre-exponential constant; $k = 0.6950348$ cm^{-1} K^{-1} is the Boltzmann constant; T is the absolute temperature, and ΔE represents the energy gap between the two-level thermal couple ($^2H_{11/2}$ and $^4S_{3/2}$). Eqn (4) can be written by taking the natural logarithm on both sides of eqn (3):

$$\ln(\mathrm{FIR}) = -\frac{\Delta E}{k}\ \frac{1}{T} + \ln A \quad (4)$$

ΔE and A parameters can be determined by using a simple linear fit of eqn (4) based on the relationship between ln(FIR) and $1/T$ (Fig. 7d).

The correlation between the calculated temperature (using the FIR) and the actual experimental temperature (read directly from the thermal coupe) has been determined using eqn (5),[13] which evaluates the reliability of the measurement, and results are shown in Fig. 7f. Fig. 7f reveals that the calculated temperature (green sphere) is consistent with the experimental temperature (red line) because of the high correlation coefficient $R^2 = 0.999$, indicating the reliability and accuracy of the FIR.

$$T = \frac{\Delta E}{k}\ \frac{1}{\ln A - \ln(\mathrm{FIR})} \quad (5)$$

Furthermore, the key parameters such as relative sensitivity (S_r) and absolute sensitivity (S_a) values can be estimated using eqn (6) and (7), respectively, to evaluate the temperature sensing performance of the resulting phosphor:[46,47]

$$S_r = \frac{1}{\mathrm{FIR}}\ \frac{d}{dT}(\mathrm{FIR}) = \frac{\Delta E}{kT^2} \quad (6)$$

$$S_a = \frac{d(\mathrm{FIR})}{dT} = \mathrm{FIR} \times \frac{\Delta E}{kT^2} \quad (7)$$

Fig. 7e shows the maximum S_r of 0.445% K^{-1} at 303 K, whereas S_a was 0.667% K^{-1} at 343 K. Moreover, the phosphor shows high-intensity emission at high temperatures (523 K), indicating its temperature stability and applicability at high temperatures.

The sensor sensitivity of the material is compared with other RE-doped phosphors to check its applicability (Table 4). As shown in Table 4, the phosphor obtained in this work has presented competitive results compared with other host lattices such as phosphate,[11,50] fluoride,[48,51] and oxide.[4,5,16,49,52] Furthermore, $CaZrO_3$:Er–Yb–Mo phosphor shows a high sensitivity temperature (0.667% K^{-1}) based on the operating temperature range (303–523 K) that is prospective for temperature sensor applications.

3.5. Downconversion luminescence properties

Fig. 8a displays the PL excitation spectra of typical samples S0 and S3. For two samples show the sharp absorption bands at

Table 4 Comparison of the sensitivity sensor of our phosphor with other phosphor based on UC emission

Sample	$S_{r\ max}$ (% K^{-1})	$S_{a\ max}$ (% K^{-1})	Temperature (K)	References
$SrWO_4$:Er, Yb	—	1.498	300–518	4
$Ba_5Y_8Zn_4O_{21}$:Er, Yb	0.39	1.36	293–563	5
$NaBiF_4$:Er, Yb, Fe	—	0.53	300–550	48
$Li_2Ti_2O_7$:Er, Yb	0.63	0.63	333–553	11
Oxyfluorotellurite glasses:Er, Yb	0.46	0.645	295–675	49
$Sr_3(PO_4)_2$:Er, Yb	0.70	0.88	303–623	50
Al_2O_3:Er, Yb, Mo	—	0.51	294–973	16
$NaGdF_4$:Er, Yb, Fe	0.27	0.78	303–523	51
$Er_{1-x}Yb_xO_3$	—	0.45	298–473	52
$CaZrO_3$:Er, Yb, Mo	0.445	0.667	303–523	This work

360 and 379 nm are assigned to the $^4I_{15/2}$–$^4G_{9/2}$ and $^4I_{15/2}$–$^4G_{11/2}$ transitions of Er^{3+} ions. Meanwhile, the doped sample (S3) shows a broad absorption band ranging from 250 to 300 nm (peak at 280 nm) corresponding to the $^1A_1$–$^3T_2$ transition of MoO_4^{2-} group involving the charge transfer state transition from O^{2-} to Mo^{6+},[53] which disappears in the undoped sample (S0). This result confirms the presence of Mo^{6+} ions in the host lattice. Notably, the absorption band intensity of sample S3 is

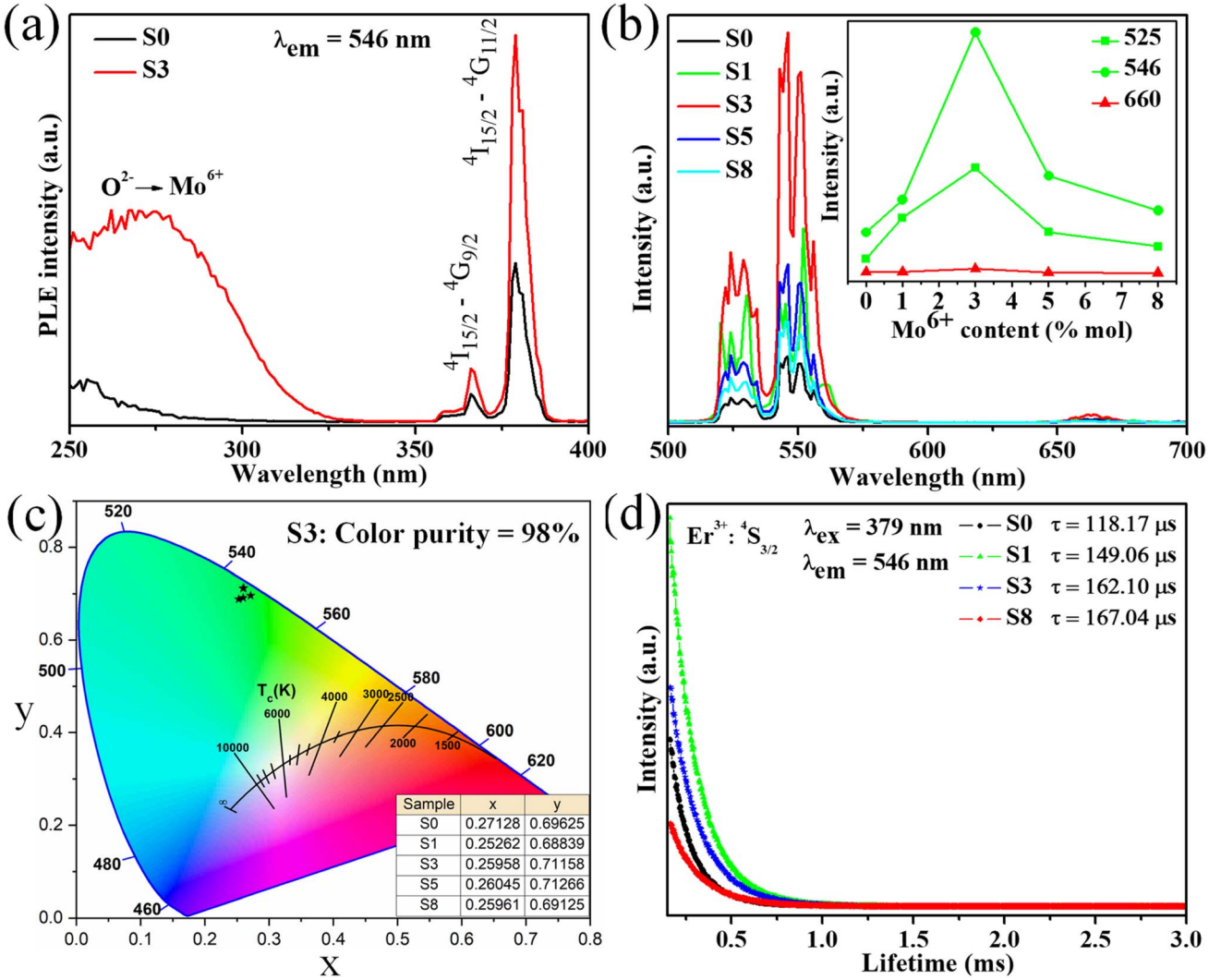

Fig. 8 (a) Excitation spectra of resulted samples, (b) down-conversion spectra of all investigated samples annealed at 1300 °C for 4 h in air and inset of the figure is dependent DC emission intensity on Mo^{6+} doping content, (c) CIE chromaticity coordinates of obtained phosphors, and (d) decay curves of all samples by monitoring $^4S_{3/2}$–$^4I_{15/2}$ transitions.

higher than the S0 sample, which could enhance the DC emission intensity of studied phosphors. Under the excitation of 379 nm, the phosphors show strong green DC emission, as shown in Fig. 8b. All samples exhibited a strong green emission at 530/546 nm and weak red emission at 660 nm, corresponding to the $^2H_{11/2}$–$^4I_{15/2}$/$^4S_{3/2}$–$^4I_{15/2}$ and $^4F_{7/2}$–$^4I_{15/2}$ transitions of Er^{3+} ions, respectively. The emission intensity of all samples increases with the enhancement of Mo^{6+} doping, reaches a maximum value with 3% mol Mo^{6+}, and then decreases with further Mo^{6+} doping content (inset of Fig. 8b). Significantly, the green emission intensity of sample S3 was six times higher than that of sample S0. The intense green UC emission of phosphor can be due to the ET from Yb^{3+}–MoO_4^{2-} dimer to Er^{3+} ions, which is similar to the enhancement mechanism of the UC emission.[23,54] By contrast, the weak red emission may correspond to the relatively small population in the $^4F_{9/2}$ level of Er^{3+} (Fig. 6). The quenching luminescence by further doping Mo^{6+} is due to cross-relaxation and ET in the Yb^{3+}–MoO_4^{2-} dimer.

Furthermore, the intensely green DC emission and weak red DC emission can be explained as follows (Fig. 6):

➢ First, the $^4I_{15/2}$ ground state of Er^{3+} ions absorb a 379 nm light excitation from the xenon lamp source and moves to the $^4G_{11/2}$ level (Fig. 6).

➢ Next, most electrons of the $^4G_{11/2}$ level NR to the $^2H_{11/2}$/$^4S_{3/2}$ level and then return to the $^4I_{15/2}$ ground state to produce two green emission bands. The intense green emission was achieved because the NR process has the fastest multi-phonon relaxation rate. Meanwhile, a few electrons are excited to the $^4I_{11/2}$ state (intermediate state of red emission), resulting in an impoverished electron population in the $^4F_{9/2}$ level, indicating fragile red emission intensity.

These results indicated that the behavior of UC and DC green emission of the $CaZrO_3$:Er–Yb–Mo phosphor was explained based on the suitably proposed mechanism because of the point of view of the electronic structure scale.

In addition, the decay curve of phosphor materials was determined to explain the DC emission mechanism of the system (including the luminescence process, type of occupancy of the dopant ion in the host lattice sites, and characterization of the luminescence center). Decay measurements of all investigated samples (S0, S1, S3, and S8) were performed using the

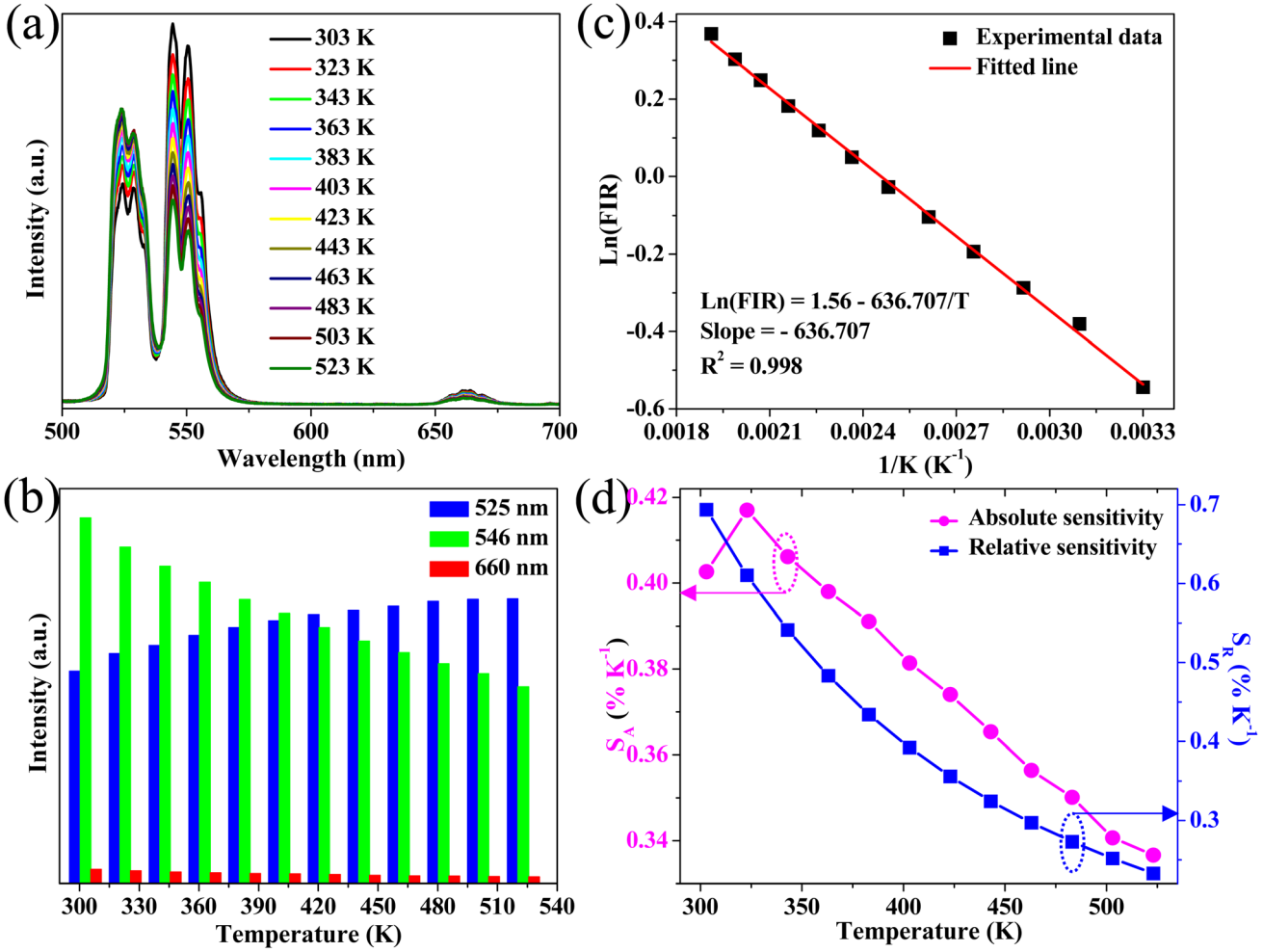

Fig. 9 (a) Photoluminescence excitation spectra of sample S3 with different temperatures ranging from 303 K to 523 K, (b) relationship between ln(FIR) and 1/*T*, (c) green and red emission intensities depend on temperature, and (d) absolute and relative sensitivities of the phosphor.

Table 5 Comparison of the sensitivity sensor of our phosphor with other phosphors based on down-conversion emission

Sample	$S_{r\ max}$ (% K^{-1})	$S_{a\ max}$ (% K^{-1})	Temperature (K)	References
Tellurite glass:Er	—	0.85	313–713	57
Germanate glass:Er	0.66	—	453–713	57
$NaGd(WO_4)_2$:Er	—	1.28	298–573	58
$NaBiTiO_3$:Er	—	0.23	80–440	59
$SrGdFGa_3O_7$:Er	—	1.06	10–430	60
$CaZrO_3$:Er, Yb, Mo	0.697	0.417	303–523	This work

379 nm excitation and 546 nm emission, as shown in Fig. 8d. The curve fitting technique can determine the lifetime of an excited state from the decay curve, which can be written as follows:[55]

$$y(t) = y_0 + Ae^{-t/\tau} \quad (8)$$

where $y(t)$ and y_0 are the intensity at time t and infinite time, respectively; A is the weighting parameter, and τ is the decay component of Er^{3+} into the host lattice. Our experimental data are correctly fitted with a single exponential, indicating the substitution of Er^{3+} ions for Ca^{2+} sites in the host lattice rather than on the particle surface.[56] The fitting results are shown in Fig. 8d. The lifetime increases (from 118.17 to 167.04 μs) with the increase of Mo^{6+}-doped content (from 0 to 8% mol), confirming the efficient ET from the Yb^{3+}–MoO_4^{2-} dimer to Er^{3+} ions. A similar phenomenon has also been observed in previous works.[5,44]

Additionally, the CIE chromaticity coordinates of DC emission samples with different Mo^{6+} doping contents were calculated, as shown in Fig. 8c. Notably, chromaticity coordinates (x, y) of the DC phosphors are most close to pure green emission. By accepting these values into eqn (2), the color purity of all samples was estimated and reached a maximum value of 98% (S3 sample), indicating the high pure green light emission of the obtained phosphor. Overall, the high color purity and long lifetime of the UC and DC phosphor suggest that it is suitable as a candidate material for optoelectronic devices.

3.6. Optical temperature sensing based on DC emission

Down-conversion emission intensities of sample S3 depending on the temperature were also investigated to estimate the temperature sensing characteristics of the phosphor, as shown in Fig. 9a. Notably, the $^2H_{11/2}$–$^4I_{15/2}$ transition intensity slightly increases with the increase of temperature. By contrast, the $^4S_{3/2}$–$^4I_{15/2}$ transition intensity significantly decreases from 303 K to 525 K (Fig. 9b). The emission intensity of the phosphor decreases with the increase of temperatures because of the thermal quenching effect.[3] Moreover, the emission intensity of the phosphor at 523 K was 54% compared with 303 K, indicating the good thermal stability of the phosphor.

Furthermore, using eqn (4) and (5), the relationship of ln(FIR) *versus* $1/T$ was determined (Fig. 9c). The fitting results shown in Fig. 9c indicate that the slope value is −636.707, corresponding to the $\Delta E/k$ value. In addition, the absolute and relative sensitivity was calculated using eqn (6) and (7) (Fig. 9d). The absolute (S_a) and relative sensitivity (S_r) maximum were 0.417% K^{-1} at 323 K and 0.697% K^{-1} at 303 K. Table 5 shows the comparison of temperature sensitivity in this work and other phosphor reported in the literature.[57–60] As shown in Table 4, the $CaZrO_3$:Er–Yb–Mo phosphor in this work has presented a competitive result. In particular, the S_r maximum value of the DC emission is higher than the UC emission because the thermal effect generated by the DC excitation source light was ignored. Therefore, the high sensing sensitivity of DC phosphor was achieved, thereby extending material's application.

4. Conclusion

The structure, morphology, and luminescent behavior of the $CaZrO_3$:Er–Yb–Mo phosphor were investigated in detail to explore their temperature sensor properties. The XRD and Rietveld refinement confirmed the formation of the orthorhombic single-phase $CaZrO_3$ with a high crystallinity degree. SEM images show a uniform cubic morphology with an average size of approximately 1 μm. The strong green UC and DC emission of the phosphor was achieved under excitation of 975 and 379 nm. Consequently, the green UC and DC emission intensities of the doped sample were increased four and sixfold, respectively, compared with the undoped sample. The ET from the high-energy excited state of the Yb^{3+}–MoO_4^{2-} dimer to the $^4F_{7/2}$ level of Er^{3+} is responsible for the enhancement of green UC and DC emissions, which is further confirmed by decay kinetics based on the DC emission of the phosphors. Additionally, the phosphor showed high green color purity, 96.50% of UC emission, and 98% of DC emission. Furthermore, the sensor sensitivity value based on DC emission was more than that of UC emission because the thermal effect generated by the DC excitation source light was ignored, thereby extending the application potential of the material. These results indicate that the $CaZrO_3$:Er–Yb–Mo phosphor is an efficient down and up-conversion luminescent material suitable for optoelectronic integrated devices and thermal sensor applications.

Author contributions

Hoang Tuan Nam: data curation, format analysis, experiment, writing – original draft. Phuong Dinh Tam: investigation, data curation. Nguyen Van Hai: methodology, format analysis. Hoang Nhu Van: conceptualization, format analysis, methodology, resources, supervision, writing – review & editing.

Conflicts of interest

The authors declare that they have no conflict of interest.

Acknowledgements

This work is funded by the Ministry of Education and Training of Vietnam, under the project B2023-SPH-06.

References

1 Y. Zhang, B. Wang, Y. Liu, G. Bai, Z. Fu and H. Liu, Upconversion luminescence and temperature sensing characteristics of Yb^{3+}/Tm^{3+}:$KLa(MoO_4)_2$ phosphors, *Dalton Trans.*, 2021, **50**, 1239–1245.

2 Y. Zhao, X. Wang, Y. Zhang, Y. Li and X. Yao, Optical temperature sensing of up-conversion luminescent materials: fundamentals and progress, *J. Alloys Compd.*, 2020, **817**, 152691.

3 Y. Wang, L. Lei, R. Ye, G. Jia, Y. Hua, D. Deng and S. Xu, Integrating Positive and Negative Thermal Quenching Effect for Ultrasensitive Ratiometric Temperature Sensing and Anti-counterfeiting, *ACS Appl. Mater. Interfaces*, 2021, **13**, 23951–23959.

4 A. Pandey, V. K. Rai, V. Kumar, V. Kumar and H. C. Swart, Upconversion based temperature sensing ability of Er^{3+}-Yb^{3+} codoped $SrWO_4$: an optical heating phosphor, *Sens. Actuators, B*, 2015, **209**, 352–358.

5 J. Chen, W. Zhang, S. Cui, X. Peng, F. Hu, R. Wei, H. Guo and D. Huang, Up-conversion luminescence properties and temperature sensing performances of $Ba_5Y_8Zn_4O_{21}$:Yb^{3+}, Er^{3+} phosphors, *J. Alloys Compd.*, 2021, **875**, 159922.

6 N. M. Bhiri, M. Dammak, M. Aguiló, F. Díaz, J. J. Carvajal and M. C. Pujol, Stokes and anti-Stokes operating conditions dependent luminescence thermometric performance of Er^{3+}-doped and Er^{3+}, Yb^{3+} co-doped $GdVO_4$ microparticles in the non-saturation regime, *J. Alloys Compd.*, 2020, **814**, 152197.

7 Ľ. Bača, H. Steiner and N. Stelzer, Upconversion luminescence and optical thermometry in Er^{3+}/Yb^{3+} co-doped CeO_2 for space application, *J. Alloys Compd.*, 2019, **774**, 418–424.

8 F. Huang, Y. Gao, J. Zhou, J. Xu and Y. Wang, Yb^{3+}/Er^{3+} co-doped $CaMoO_4$: a promising green upconversion phosphor for optical temperature sensing, *J. Alloys Compd.*, 2015, **639**, 325–329.

9 S. A. Wade, S. F. Collins and G. W. Baxter, Fluorescence intensity ratio technique for optical fiber point temperature sensing, *J. Appl. Phys.*, 2003, **94**, 4743–4756.

10 P. Singh, R. S. Yadav, P. Singh and S. B. Rai, Upconversion and downshifting emissions of Ho^{3+}-Yb^{3+} co-doped $ATiO_3$ perovskite phosphors with temperature sensing properties in Ho^{3+}-Yb^{3+} co-doped $BaTiO_3$ phosphor, *J. Alloys Compd.*, 2021, **855**, 157452.

11 Y. Liu, G. X. Bai, E. Pan, Y. J. Hua, L. Chen and S. Q. Xu, Upconversion fluo-rescence property of Er^{3+}/Yb^{3+} co-doped lanthanum titanate micro- crystals for optical thermometry, *J. Alloy. Compd.*, 2020, **822**, 153449.

12 O. Kıbrıslı, E. Erol, N. Vahedigharehchopogh, E. S. Yousef, M. Ç. Ersundu and A. E. Ersundu, Noninvasive optical temperature sensing behavior of Ho^{3+} and Ho^{3+}/Er^{3+} doped tellurite glasses through up and down-converted emissions, *Sens. Actuators, A*, 2020, **315**, 112321.

13 C. V. Thai, N. T. Dung, N. V. Hai, V. T. N. Minh, N. X. Truong, P. A. Tuan, P. V. Huan and H. N. Van, Intense green upconversion emission of rare-earth-doped $Sr_3(PO_4)_2$/$Sr_2P_2O_7$ powder: effect of annealing temperature and temperature-sensor properties, *Optik*, 2022, **264**, 169446.

14 W. Ge, M. Xu, J. Shi, J. Zhu and Y. Li, Highly temperature-sensitive and blue upconversion luminescence properties of $Bi_2Ti_2O_7$:Tm^{3+}/Yb^{3+} nanofibers by electrospinning, *Chem. Eng. J.*, 2020, **391**, 123546.

15 B. S. Cao, Y. Y. He, Z. Q. Feng, Y. S. Li and B. Dong, Optical temperature sensing behavior of enhanced green upconversion emissions from Er-Mo:$Yb_2Ti_2O_7$ nanophosphor, *Sens. Actuators, B*, 2011, **159**, 8–11.

16 B. Dong, B. S. Cao, Z. Q. Feng, X. J. Wang and Y. Y. He, Optical temperature sensing through extraordinary enhancement of green up-conversion emissions for Er-Yb-Mo:Al_2O_3, *Sens. Actuators, B*, 2012, **165**, 34–37.

17 B. Dong, B. Cao, Y. He, Z. Liu, Z. Li and Z. Feng, Temperature sensing and *in vivo* imaging by molybdenum sensitized visible upconversion luminescence of rare-earth oxides, *Adv. Mater.*, 2012, **24**, 1987–1993.

18 X. Yang, Z. Fu, Y. Yang, C. Zhang, Z. Wu and T. Sheng, Optical Temperature Sensing Behavior of High-Efficiency Upconversion: Er^{3+}-Yb^{3+} Co-Doped $NaY(MoO_4)_2$ Phosphor, *J. Am. Ceram. Soc.*, 2015, **98**, 2595–2600.

19 A. A. Ansari, A. K. Parchur, M. Alam and A. Azzeer, Structural and photoluminescence properties of Tb-doped $CaMoO_4$ nanoparticles with sequential surface coatings, *Mater. Chem. Phys.*, 2014, **147**, 715–721.

20 H. N. Van, M. T. Y. Thanh, P. H. Vuong, P. V. Huan, V. T. N. Minh, P. A. Tuan and T. D. Hien, Experimental and theoretical studies of red emission enhancing mechanism in Al-doped $CaMoO_4$:Eu phosphor, *Opt. Mater.*, 2022, **132**, 112831.

21 H. N. Van, V. N. Hung, P. H. Vuong, P. V. Huan, B. T. Hoan, N. D. Hung and L. M. Tu, A novel upconversion emission material based on Er^{3+} - Yb^{3+} - Mo^{6+} tridoped hydroxyapatite/tricalcium phosphate (HA/β-TCP), *J. Alloys Compd.*, 2020, **827**, 154288.

22 H. N. Van, L. M. Tu, D. T. T. Dung, P. H. Vuong, N. D. Hung, P. T. H. Diep and H. V. Hung, On enhancement and control of green emission of rare earth co-doped hydroxyapatite nanoparticles: synthesis and upconversion luminescence properties, *New J. Chem.*, 2021, **45**, 751–760.

23 D. T. T. Dung, V. T. N. Minh, N. X. Truong, P. V. Huan, P. H. Vuong, N. D. Hung, B. T. Hoan, L. M. Tu and H. N. Van, Dual-mode green emission and temperature sensing properties of rare-earth-element-doped biphasic calcium phosphate composites, *J. Alloys Compd.*, 2021, **871**, 159483.

24 J. L. Wu, B. S. Cao, F. Lin, B. J. Chen, J. S. Sun and B. Dong, A new molybdate host material: synthesis, upconversion, temperature quenching and sensing properties, *Ceram. Int.*, 2016, **42**, 18666–18673.

25 K. Shan, F. Zhai, Z. Z. Yi, X. T. Yin, D. Dastan, F. Tajabadi, A. Jafari and S. Abbasi, Mixed conductivity and the conduction mechanism of the orthorhombic $CaZrO_3$ based materials, *Surf. Interfaces*, 2021, **23**, 100905.

26 A. Maurya, A. Dwivedi, A. Bahadur and S. B. Rai, Enhanced upconversion and downshifting emissions from Tm^{3+}, Yb^{3+} co-doped $CaZrO_3$ phosphor in the presence of alkali ions (Li^+, Na^+ and K^+), *J. Alloys Compd.*, 2019, **786**, 457–467.

27 A. Khan, F. Song, X. Gao, Z. Chen, X. Sang, M. Feng and L. Liu, Introduction of Molybdenum into the lattice of single-host $CaZrO_3$: Dy^{3+}/Eu^{3+} to enhance luminescence intensity of the phosphor for white light emission, *J. Alloys Compd.*, 2021, **881**, 160652.

28 V. Singh, V. Kumar Rai and M. Haase, Intense green and red upconversion emission of Er^{3+},Yb^{3+} co-doped $CaZrO_3$ obtained by a solution combustion reaction, *J. Appl. Phys.*, 2012, **112**, 1–6.

29 A. Maurya, A. Bahadur and S. B. Rai, Enhanced red emission from Eu^{3+}, A^+ (Li^+, Na^+, K^+) co-doped $CaZrO_3$ phosphor, *J. Lumin.*, 2018, **203**, 714–722.

30 D. Navamia, G. P. Darshan, D. R. Lavanya, H. B. Premkumar, S. C. Sharma, H. Adarsha, H. C. Prameela and H. Nagabhushan, Design of green emitting $CaZrO_3$:Tb^{3+} nanophosphor: luminescence based platform for real-time ultrasensitive detection of latent fingerprints and anti-counterfeiting applications, *Opt. Mater.*, 2021, **122**, 111474.

31 A. Khan, F. Song, A. Zhou, X. Gao, M. Feng, M. Ikram, H. Hu, X. Sang and L. Liu, Tuning white light upconversion emission from Yb^{3+}/Er^{3+}/Tm^{3+} triply doped $CaZrO_3$ by altering Tm^{3+} concentration and excitation power, *J. Alloys Compd.*, 2020, **835**, 155286.

32 Y. Hua and J. S. Yu, Strong Green Emission of Erbium(III)-Activated La_2MgTiO_6 Phosphors for Solid-State Lighting and Optical Temperature Sensors, *ACS Sustainable Chem. Eng.*, 2021, **9**, 5105–5115.

33 H. N. Van, P. D. Tam, P. H. Vuong, N. D. Hung, C. X. Thang and L. Q. Minh, Control of red upconversion emission in Er^{3+}–Yb^{3+}– Fe^{3+} tri–doped biphasic calcium phosphate, *Inorg. Chem. Commun.*, 2023, **150**, 110538.

34 K. Singh, M. Rajendran, R. Devi and S. Vaidyanathan, Narrow-band red-emitting phosphor with negligible concentration quenching for hybrid white LEDs and plant growth applications, *Dalton Trans.*, 2021, **50**, 4986.

35 L. Li, W. Chang, J. He, Y. Yan, M. Cui, S. Jiang, G. Xiang and X. Zhou, Molybdenum substitution simultaneously induced band structure modulation and luminescence enhancement in LiLaMg(W, Mo)O_6:Eu^{3+} red-emitting phosphor for near ultraviolet excited white light diodes, *J. Alloys Compd.*, 2018, **763**, 278–288.

36 M. Pal, U. Pal, J. M. G. Y. Jiménez and F. Pérez-Rodríguez, Effects of crystallization and dopant concentration on the emission behavior of TiO_2: Eu nanophosphors, *Nanoscale Res. Lett.*, 2012, **7**, 1–12.

37 Y. Y. He, X. L. Liu, B. S. Cao, Z. Q. Feng and B. Dong, A general approach for selective enhancement of green upconversion emissions in Er^{3+} doped oxides by Yb^{3+}-MoO_4^{2-} dimer sensitizing, *J. Sol-Gel Sci. Technol.*, 2013, **66**, 312–316.

38 X. Bao, S. Zhou, J. Wang, L. Zhang, S. Huang and Y. Pan, Color tunable phosphor $CaMoO_4$:Eu^{3+}, Li^+ *via* energy transfer of MoO_4^{2-}–Eu^{3+} dependent on morphology and doping concentration, *Mater. Res. Bull.*, 2013, **48**, 1034–1039.

39 J. Sun, F. Lai, L. Ke, J. Chen, X. Shi, Y. Qiang and W. You, Upconversion luminescence of $La_4Ti_9O_{24}$: Er–Yb phosphor with high green color purity, *Opt. Mater.*, 2023, **138**, 113656.

40 B. Su, H. Xie, Y. Tan, Y. Zhao, Q. Yang and S. Zhang, Luminescent properties, energy transfer, and thermal stability of double perovskites La_2MgTiO_6:Sm^{3+}, Eu^{3+}, *J. Lumin.*, 2018, **204**(1028), 457–463.

41 W. Zheng, B. Sun, Y. Li, T. Lei, R. Wang and J. Wu, Low Power High Purity Red Upconversion Emission and Multiple Temperature Sensing Behaviors in Yb^{3+},Er^{3+} Codoped Gd_2O_3 Porous Nanorods, *ACS Sustainable Chem. Eng.*, 2020, **8**, 9578–9588.

42 J. Chen, W. Zhang, S. Cui, X. S. Peng, F. F. Hu, R. F. Wei, H. Guo and D. X. Huang, Up-conversion luminescence properties and temperature sensing performances of $Ba_5Y_8Zn_4O_{21}$:Yb^{3+}, Er^{3+} phosphors, *J. Alloys Compd.*, 2021, **875**, 159922.

43 Y. Cong, B. Dong, N. Yu, Y. He, Y. Zhao and Y. Yang, Enhanced upconversion emission in ZrO_2-Al_2O_3 composite oxide, *Dalton Trans.*, 2016, **45**, 6627–6633.

44 D. K. Singh and J. Manam, Efficient dual emission mode of green emitting perovskite $BaTiO_3$: Er^{3+} phosphors for display and temperature sensing applications, *Ceram. Int.*, 2018, **44**, 10912–10920.

45 B. Hou, M. Jia, P. Li, G. Liu, Z. Sun and Z. Fu, Multifunctional Optical Thermometry Based on the Rare-Earth-Ions-Doped Up-/Down-Conversion $Ba_2TiGe_2O_8$:Ln (Ln = Eu^{3+}/Er^{3+}/Ho^{3+}/Yb^{3+}) Phosphors, *Inorg. Chem.*, 2019, **58**, 7939–7946.

46 K. M. Krishna, S. P. Tiwari, A. Kumar and K. Kumar, Up- and downconversion emission studies in Er^{3+}/Yb^{3+}: $Ca_3(PO_4)_2$ phosphor for thermometry, *Sens. Actuators, A*, 2020, **315**, 112302.

47 W. Zhang, X. Huang, W. Liu, Z. Gao, L. Zhong, Y. Qin, B. Li and J. Li, Semiconductor Plasmon Enhanced Upconversion toward a Flexible Temperature Sensor, *ACS Appl. Mater. Interfaces*, 2023, **15**, 4469–4476.

48 P. Du, Q. Zhang, X. Wang, L. Luo and W. Li, Upconversion luminescence, temperature sensing and internal heating behaviors of Er^{3+}/Yb^{3+}/Fe^{3+}-tridoped $NaBiF_4$ nanoparticles, *J. Alloys Compd.*, 2019, **805**, 171–179.

49 R. Lisiecki, M. Lukaszewicz, B. Klimesz and W. R. Romanowski, Er^{3+},Yb^{3+}-doped oxyfluorotellurite glasses—Impact of temperature on spectroscopic properties and optical sensor qualities, *J. Non-Cryst. Solids*, 2020, **535**, 119965.

50 T. Zheng, L. Zhou, X. Qiu, D. Yang, M. Runowski, S. Lis, P. Du and L. Luo, Er^{3+}/Yb^{3+} co-doped $Sr_3(PO_4)_2$ phosphors:

a ratiometric luminescence thermometer based on Stark levels with tunable sensitivity, *J. Lumin.*, 2020, **227**, 117517.

51 J. Tang, P. Du, W. Li and L. Luo, Boosted thermometric performance in $NaGdF_4$:Er^{3+}/Yb^{3+} upconverting nanorods by Fe^{3+} ions doping for contactless nanothermometer based on thermally and non-thermally coupled levels, *J. Lumin.*, 2020, **224**, 117296.

52 K. Feng, B. Lu and L. Hu, Down/Upconversion Luminescence Behaviors and Temperature-Sensing Properties of Highly Transparent $(Er_{1-x}Yb_x)_2O_3$ Ceramics, *ACS Appl. Electron. Mater.*, 2022, **4**(2), 761–767.

53 F. Kang, M. Peng, S. Xu, Z. Ma, G. Dong and J. Qiu, Broadly Tunable Emission from $CaMoO_4$:Bi Phosphor Based on Locally Modifying the Microenvironment Around Bi^{3+} Ions, *Eur. J. Inorg. Chem.*, 2014, **8**, 1373–1380.

54 S. Fan, S. Wang, H. Sun, S. Sun, G. Gao and L. Hu, Efficient dual-mode up-conversion and down-shifting emission in β-$NaYF_4$:Yb^{3+},Er^{3+} microcrystals *via* ion exchange, *J. Am. Ceram. Soc.*, 2017, **100**, 3061–3069.

55 J. Mu, W. Sun, F. Li, Y. Guan, X. Zhou, J. Li and L. Chen, Upconversion luminescent perovskite $CaTiO_3$:Yb^{3+}/Er^{3+} nanocubes, *J. Alloys Compd.*, 2019, **797**, 1002–1006.

56 A. Kumar and J. Manam, Optical thermometry using up and down conversion photoluminescence mechanism in $Y_2Zr_2O_7$:Er^{3+} phosphors with excellent sensing sensitivity, *J. Alloys Compd.*, 2020, **829**, 154610.

57 G. Z. Sui, X. P. Li, L. H. Cheng, J. S. Zhang, J. S. Sun, H. Y. Zhong, Y. Tian, S. B. Fu and B. J. Chen, Laser cooling with optical temperature sensing in Er^{3+}-doped tellurite-germanate glasses, *Appl. Phys. B: Lasers Opt.*, 2013, **110**, 471–476.

58 X. Ming, Q. Meng, S. Lü and W. Sun, The hydrothermal synthesis and morphology-dependent optical temperature sensing properties of Er^{3+} doped $NaGd(WO_4)_2$ phosphor, *J. Lumin.*, 2017, **192**, 196–202.

59 S. Wang, S. Zheng, H. Zhou, A. Pan, G. Wu and J. M. Liu, Down-conversion luminescence and its temperature-sensing properties from Er^{3+}-doped sodium bismuth titanate ferroelectric thin films, *Appl. Phys. A: Mater. Sci. Process.*, 2015, **121**, 773–777.

60 H. X. Sun, N. Yuan, D. Y. Liu, Z. B. Zhang, Y. Wang, W. H. Wong, D. Y. Yu, E. Y. B. Pun and D. L. Zhang, A simple, low-cost, highly efficient optical thermometry based on down-conversion green fluorescence of Er^{3+}:$SrGdGa_3O_7$ crystal, *Mater. Res. Bull.*, 2017, **94**, 408–414.